文章编号: 1001 - 9014(2016)06 - 0676 - 05
DOI:10.11972/j.issn.1001 - 9014.2016.06.08

The structural and optical properties of $Zn_x Ni_{(1-x)} Mn_2 O_4$ films grown on $Pt/Ti/SiO_2/Si$ substrate

WANG Wan-Sheng[1,2], HOU Yun[1*], ZHANG Zeng-Hui[3], ZHOU Wei[1],
GAO Yan-Qing[1], WU Jing[1], CHU Jun-Hao[1]

(1. National Laboratory for Infrared Physics, Shanghai Institute of Technical Physics, Chinese Academy of Sciences, Shanghai 200083, China; 2. University of Chinese Academy of Sciences, Beijing 100049, China; 3. School of Material Science and Engineering, University of Shanghai for Science and Technology, Shanghai 200093, China)

Abstract: The spinel oxide $Zn_xNi_{1-x}Mn_2O_4$ (ZNMO, $x=0$, 0.05, 0.1, 0.15, 0.2, 0.25) films have been grown on $Pt/Ti/SiO_2/Si$ substrate by chemical solution deposition (CSD) method. The crystallization and microstructural features of ZNMO films are studied by x-ray diffraction (XRD) and field-emission scanning electron microscopy (FESEM) analysis, respectively. The results show that the structural property of ZNMO films is affected by Zn concentration. The optical constants of ZNMO films have been analyzed by spectroscopic ellipsometry measurements in the wavelength range of 300-1 100 nm. The changes of the refractive index n and extinction coefficient k caused by Zn substituting are discussed. The A_{1g} and F_{2g} modes have been observed in Raman spectra. The relative intensity of the A_{1g} mode decreases with increasing Zn concentration. The Raman peak positions shift slightly with Zn concentration x, which might result from lattice strain and lattice mismatch.

Key words: spinel oxide, structural property, optical constants, Raman spectra
PACS: 78. 20. -e, 68. 55. -a

生长于 $Pt/Ti/SiO_2/Si$ 衬底的 $Zn_x Ni_{(1-x)} Mn_2 O_4$ 薄膜的结构与光学性质

王万胜[1,2], 侯 云[1*], 张增辉[3], 周 炜[1], 高艳卿[1], 吴 敬[1], 褚君浩[1]
(1. 中国科学院上海技术物理研究所 红外物理国家重点实验室,上海 200083;
2. 中国科学院大学,北京 100049;
3. 上海理工大学 材料科学与工程学院,上海 200093)

摘要:采用化学溶液法在 $Pt/Ti/SiO_2/Si$ 衬底上生长了 $Zn_xNi_{1-x}Mn_2O_4$ (ZNMO, $x=0$, 0.05, 0.1, 0.15, 0.2, 0.25)尖晶石氧化物薄膜。X 射线衍射(XRD)与场发射扫描电子显微镜(FESEM) 分析结果表明,Zn 的掺杂浓度对 ZNMO 薄膜的结晶性和微结构有明显影响。用椭圆偏振光谱仪测量分析了 ZNMO 薄膜在 300-1 100 nm 波段的光学常数,并讨论了 Zn 掺杂对折射率 n 和消光系数 k 的影响。在薄膜的拉曼光谱中观测到两个峰 A_{1g} 与 F_2g,A_{1g}模式的相对峰位随着 Zn 的掺杂浓度 x 的增大而减小。由于晶格应变与晶格失配,拉曼峰峰位随 Zn 掺杂浓度的变化而轻微移动。

关 键 词:尖晶石氧化物;结构特性;光学常数;拉曼光谱
中图分类号:O484.1;O484.4+1 **文献标识码**:A

Introduction

In the past decades, the $NiMn_2O_4$ system with the general formula AB_2O_4 has been one of the most important thermistor materials because of the excellent negative temperature coefficients (NTC) [1-4]. For normal spinel

Received date: 2016-03-25, **revised date**: 2016-09-28 **收稿日期**:2016-03-25, **修回日期**:2016-09-28
Foundation items:Supported by National Natural Science Foundation of China(61275111, 11304336), Shanghai Project (15ZR1445700)
Biography:WANG Wan-Sheng(1990-), male, Henan China, Master. Research area involves the structural, optical and electrical Properties of Mn-Co (Zn)-Ni-O Films. E-mail:wangwsh@shanghaitech.edu.cn
* **Corresponding author**:E-mail: hyun@mail.sitp.ac.cn

structure $[A]^{tet}[B_2]^{oct}O_4$, the tetrahedral sites are occupied by A ions and octahedral sites are occupied by B ions. However, for $NiMn_2O_4$, the spinel structure has been observed as "intermediate" (partially inverse) whose formula is given by $[B_\nu A_1\text{-}\nu]^{tet}[A_\nu B_2\text{-}\nu]^{oct}O_4$, where ν is the inversion parameter and its value is between 0 and 1 [5-6]. For the inverse spinel ($\nu=1$), B ions occupy the tetrahedral sites entirely, both A and B ions are located at the octahedral sites. The material properties are closely linked with the variant cations in the tetrahedral and octahedral sites [5, 7-8]. Owing to the effects of cation distribution on the physical properties, substituting A or B ions by other elements is an effective method to induce significant variation of the structural, electrical, magnetic and optical properties of the materials[9-13]. Recently some researches indicated that substitution of nickel ions by zinc ions can improve the electrical stability effectively and have low resistivity in some particular compositions for the Zn-Ni-Mn-O system materials[14-15]. Although some physical properties of Zn-Ni-Mn-O ternary spinel system have been widely studied, the ceramic samples are normally fabricated from powders by high temperature sintering method and few studies about the performance of Zn-Ni-Mn-O films have been reported[16-18]. The film of materials have high density and stability due to low porosity, which can be used for the thermal device with the modern integrated technology[1]. Furthermore, the optical properties of the Zn-Ni-Mn-O system film can be well investigated, which is very important in the application of thermistor materials and optoelectronic devices[19].

In our research, the $Zn_xNi_{1-x}Mn_2O_4$ (ZNMO) (x = 0, 0.05, 0.1, 0.15, 0.2, 0.25) films were fabricated by chemical solution deposition (CSD) method. The optical constants were analyzed by spectroscopic ellipsometry (SE) spectra. A four layer model (air/rough layer/ZNMO/Pt) has been used to fit the experimental data and the ZNMO films are represented by the double Tauc-Lorentz (DTL) oscillators. Variations of the optical properties and the Raman spectra of the ZNMO films were investigated in detail.

1 Experimental

The ZNMO (x = 0, 0.05, 0.1, 0.15, 0.2, 0.25) films were prepared on $Pt(111)/Ti/SiO_2/Si$ substrate by CSD method. The original materials were zinc acetate, nickel acetate and manganese acetate. The acetates were dissolved into glacial acetic acid with the atom ratios of Zn:Ni:Mn = 0:1:2, 0.05:0.95:2, 0.1:0.9:2, 0.15:0.85:2, 0.2:0.8:2 and 0.25:0.75:2. Then the mixtures were filtered through 0.2 μm syringe filters to remove the dust and impurities. The solutions were green and transparent. The films were deposited on $Pt(111)/Ti/SiO_2/Si$ substrate by spin coating at 4000 rpm for 20 s. After coating each layer, the wet films were dried at 250 °C to remove residual organic, followed by annealing at 750 °C. The deposition and heat-treatment procedure were then repeated for fifty times to obtain the film with a desired thickness.

The phase analysis of the films was identified by x-ray diffraction (XRD) using a Rigaku D/MAX-2550 x-ray diffractometer at room temperature (RT). The surface morphology was observed by FEI (Sirion 200) field-emission scanning electron microscopy (FESEM). The optical properties were investigated in the wavelength range of 300 ~ 1100 nm under the incident angle of 60° by ultraviolet-near-infrared SE (SC620 by Shanghai Sanco, Inc.). The RT micro-Raman scattering experiments were performed in a qusai-backscattering geometry using the 514.5 nm line of an Ar-ion laser and the scattering signal was collected by Tri-Vista Triple Raman Spectroscopy equipped with a liquid-nitrogen cooled charge coupled device detector.

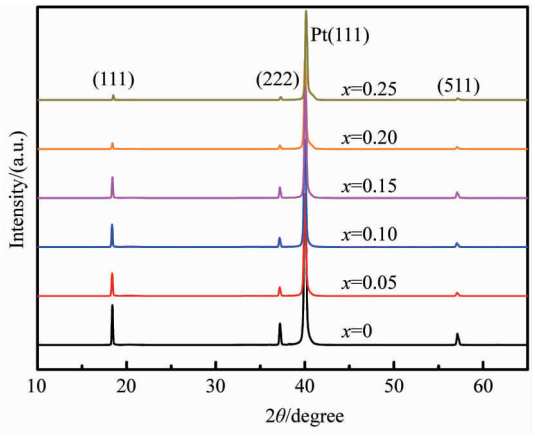

Fig. 1　XRD patterns of the ZNMO (x = 0, 0.05, 0.1, 0.15, 0.2 and 0.25) films

图 1　ZNMO (x = 0, 0.05, 0.1, 0.15, 0.2, 0.25) 薄膜的 XRD 图谱

2 Results and discussion

Figure 1 shows the XRD patterns of the ZNMO (x = 0, 0.05, 0.1, 0.15, 0.2, 0.25) films deposited on $Pt/Ti/SiO_2/Si$ substrate by CSD method. The diffraction positions are confirmed by the JCPDS data cards No. 84-0542 for $NiMn_2O_4$. The intensities of (111), (222) and (511) peaks increase with the decrease of Zn concentration, which is due to the crystal growth and improvement of crystallization. In addition, $NiMn_2O_4$ (x = 0) has the best crystallization compared with the films doped by zinc element and all the samples have (111) highly preferred orientation. The lattice constant a of the ZNMO (x = 0, 0.05, 0.1, 0.15, 0.2, 0.25) films are 8.34, 8.35, 8.36, 8.32, 8.34, 8.30Å, respectively. It can be seen that the lattice constant increases when the Zn concentration increases from 0 to 0.1. The substitution of Zn for Ni in $NiMn_2O_4$ expands the spinel lattice, which is explained by the larger ionic radius of Zn^{2+} (0.58 Å) as compared with ionic radius of Ni^{2+} (0.565 Å). As the Zn concentration x is up to 0.15, the values of the lattice constant do not increase with increasing Zn concentration. The phenomenon has also been observed in Zn-Ni-Mn-O ceramic materials, which can be explained by the change of cation distribution in the tetrahedral and octahedral sites [14]. It was reported that all Zn^{2+} ions occupy the tetrahedral sites in the spinel struc-

ture [5, 20]. When the Zn^{2+} concentration x is close to or greater than 1-ν (ν is in the range of 0.87 to 0.8 with temperature increasing from 115 K to RT [5-6]), the cation reconfiguration between the tetrahedral and octahedral sites arises in a great degree, which is not enough to generate the tetragonal spinel phase. All the samples of $Zn_xNi_{1-x}Mn_2O_4$ (x = 0, 0.05, 0.1, 0.15, 0.2, 0.25) films show the pure cubic spinel structure.

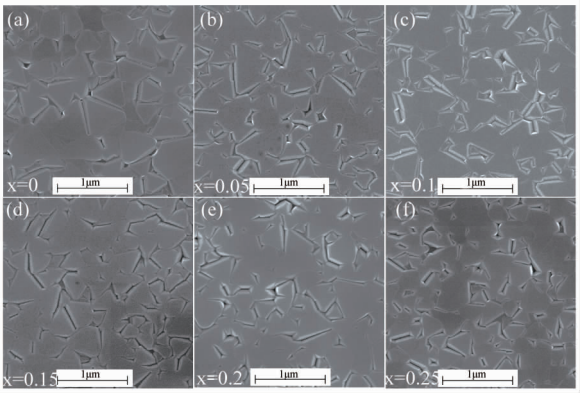

Fig. 2 (a)-(f) FESEM images of the ZNMO films for x = 0, 0.05, 0.1, 0.15, 0.2 and 0.25, respectively
图2 (a)-(f) 分别为 ZNMO (x = 0, 0.05, 0.1, 0.15, 0.2, 0.25) 薄膜的 FESEM 图片

The FESEM images of the ZNMO films are shown in Figs. 2(a)-(f) for x = 0, 0.05, 0.1, 0.15, 0.2 and 0.25, respectively. It is clear that the grain size of $NiMn_2O_4$ (x = 0) is larger than that of Zn-substituted samples which have more grain boundaries. There is no obvious variation among the surfaces of the Zn-substituted samples and they have similar surface morphology. The observation of surface roughness by the FESEM images is essential for the analysis of SE spectra.

The air/rough layer/ZNMO/Pt model has been used to analyze the SE spectra. The rough layer is described in terms of Bruggeman Effective Medium Approximation (EMA) and the dielectric function of the serial films is represented by the DTL dispersion [21-23]. The refractive index n and extinction coefficient k are obtained from the following equation:

$$n = \frac{1}{\sqrt{2}}\sqrt{\sqrt{\varepsilon_1^2+\varepsilon_2^2}+\varepsilon_1} \quad , \quad (1)$$

$$k = \frac{1}{\sqrt{2}}\sqrt{\sqrt{\varepsilon_1^2+\varepsilon_2^2}-\varepsilon_1} \quad . \quad (2)$$

The real part ε_1 is calculated by kramers-kroning integration:

$$\varepsilon_1 = \varepsilon_\infty + \frac{2}{\pi}P\int_{E_g}^{\infty}\frac{\xi\varepsilon_2(E)}{\xi^2-E^2}\mathrm{d}\xi \quad , \quad (3)$$

p represents the Cauchy principal part of the integral and ε_∞ is the high frequency dielectric constant.

The imaginary part ε_2 can be described by the DTL dispersion formula:

$$\varepsilon_2(E) = \begin{cases} \sum_{i=1}^{2}\dfrac{A_iE_{0i}C_i(E-E_{gi})^2}{(E^2-E_{0i}^2)^2+C_iE^2}\dfrac{1}{E} & E > E_g \\ 0 & E \leqslant E_g \end{cases} . \quad (4)$$

The equation contains four parameters: transition matrix element A_i, peak transition energy E_{0i}, broadening term C_i and band gap E_{gi}.

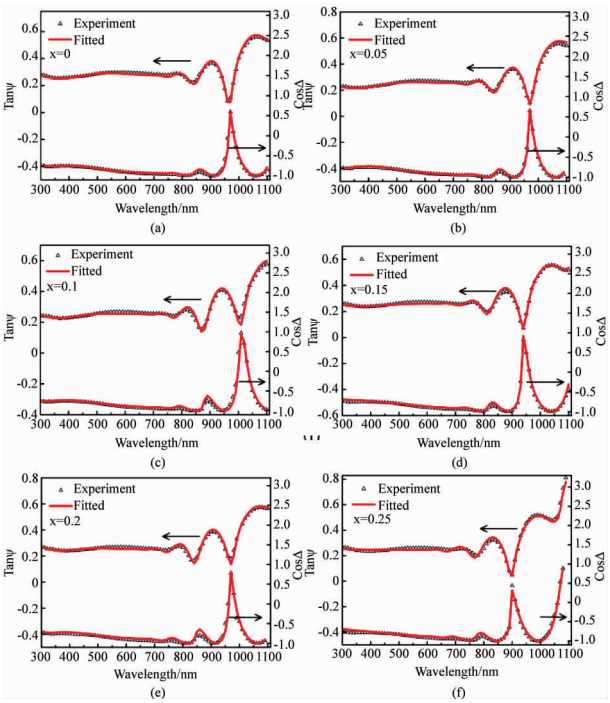

Fig. 3 (a)-(f) The experimental (triangles) and fitted (solid lines) ellipsometric spectra tanΨ and cosΔ of the ZNMO films at the incident angle 60° for x = 0, 0.05, 0.1, 0.15, 0.2 and 0.25, respectively
图3 (a)-(f) 分别为当 x = 0, 0.05, 0.1, 0.15, 0.2, 0.25, 入射角为 60° 时 ZNMO 薄膜的椭偏光谱 tanΨ 和 cosΔ 的实验值(三角形)与拟合值(实线)

Table 1 The measured-thickness and parts of parameters values of DTL model for the ZNMO films
表1 ZNMO 薄膜的测量厚度与部分 DTL 模型的参数值

Sample (x)	0	0.05	0.1	0.15	0.20	0.25
Measured-thickness /nm	950	1 040	1 050	1 020	1 040	977
Fitted-thickness /nm	951.3	1 039.8	1 058.3	1 012.7	1 034.2	982.8
Roughness /nm	42.8	38.7	39.6	25.4	35.5	24.8
f_v/(%)	15.5	12.9	17.5	21.8	18.6	22
E_{01}/eV	2.32	2.35	2.47	2.25	2.64	2.84

The experimental data has been fitted by the air/rough layer/ZNMO/Pt model, the measured-thickness and part of parameters values of DTL model for the ZNMO (x = 0, 0.05, 0.1, 0.15, 0.2, 0.25) films are shown in Table 1. The measured-thicknesses were obtained by FESEM for comparison. The fitted-thicknesses are in reasonable agreement with the measured-thicknesses. Figures 3(a)-(f) shows the experimental and fitted data tanΨ and cosΔ of the ZNMO films at the incident angle 60° in the wavelength range of 300 ~ 1100 nm for x = 0, 0.05, 0.1, 0.15, 0.2, 0.25, respectively. It can be seen that the model-based calculations fit quite well with the measured spectra for all the samples. The refractive index n and extinction coefficient κ of the ZNMO

($x=0$, 0.05, 0.1, 0.15, 0.2, 0.25) films are shown in Fig. 4.

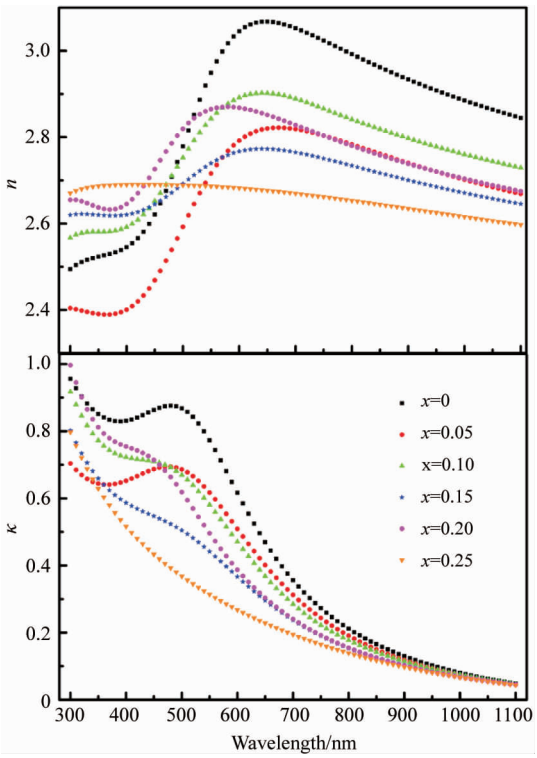

Fig. 4　The Refractive index n and extinction coefficient κ of the ZNMO ($x=0$, 0.05, 0.1, 0.15, 0.2, 0.25) films
图 4　ZNMO ($x=0$, 0.05, 0.1, 0.15, 0.2, 0.25) 薄膜的折射率 n 与消光系数 κ

It is well known that crystallinity, electronic band structure and lattice defect are important parameters, which can influence the optical constants. Owning to Zn substituting, the electronic band structure is affected and thus can further influence the optical responses of ZNMO films[14, 24]. As shown in Fig. 4, the refractive index n increases with increasing Zn concentration from 0.05 to 0.25 in the wavelength range of 300 ~ 440 nm. Besides the effect of electronic band, crystallinity is also a crucial parameter. That is why the refractive index of $NiMn_2O_4$ ($x=0$) is the largest among all the samples in the wavelength range of 510 ~ 1 100 nm[25-26]. The thicknesses of the films also make a difference in the refractive index[27]. All the factors mentioned above result in that the refractive index changes erratically with increasing Zn concentration in the wavelength range of 300-1 100 nm. For the extinction coefficient κ, the peaks in curves of the samples ($x=0$, 0.05, 0.1, 0.15 and 0.2) indicate strong optical absorption, which might be resulted from electronic transition. The values of peak transition energy E_{01} evaluated by DTL model are shown in Table 1. In the wavelength range of 500 ~ 900 nm, the extinction coefficient k decreases with increasing Zn concentration except $x=0.2$. The extinction coefficient is near zero and all the films are almost transparent in the wavelength range of 900 ~ 1 100 nm.

Fig. 5 shows the Raman spectra of the ZNMO ($x=0$, 0.05, 0.1, 0.15, 0.2, 0.25) films performed at room temperature. The Raman bands near the 643 cm^{-1} and 513 cm^{-1} are assigned as the A_{1g} and F_{2g} modes, respectively. The A_{1g} mode attributes to the symmetric Mn^{3+}-O stretching vibration in the MnO_6 bonding, and the F_{2g} mode is from the symmetric Mn^{4+}-O bending vibration[28-30]. As the Zn concentration increases, the relative intensity of the A_{1g} mode decreases, while the relative intensity of the F_{2g} mode does not change. This means that the concentration of Mn^{3+} decreases, while the concentration of Mn^{4+} remains unchanged. The Raman peaks of the Zn-substituted samples shift towards high frequency compared with the $NiMn_2O_4$ ($x=0$) film. The peaks of ZNMO films shift slightly when the Zn concentration increases from 0.05 to 0.25. This might be caused by the change of stress which is compromise of interaction among the lattice strain owing to Zn substituting, lattice mismatch and the differences in the film thickness[31-33]. The investigations of the Raman spectra prove that cation configuration and lattice deformation are related to the Zn concentration.

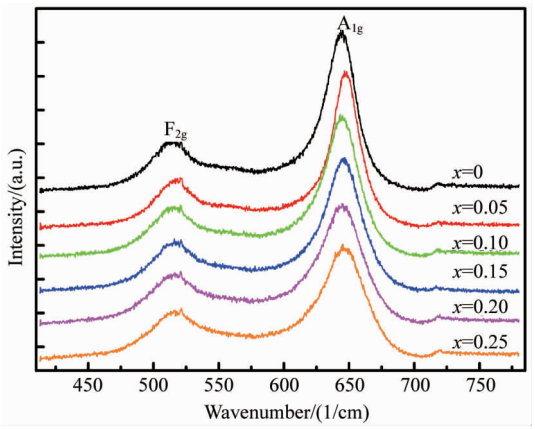

Fig. 5　The Raman spectra of the ZNMO ($x=0$, 0.05, 0.1, 0.15, 0.2 and 0.25) films
图 5　ZNMO ($x=0$, 0.05, 0.1, 0.15, 0.2, 0.25) 薄膜的拉曼光谱图

3　Conclusion

In summary, the structural and optical properties of the ZNMO ($x=0$, 0.05, 0.1, 0.15, 0.2, 0.25) films on $Pt/Ti/SiO_2/Si$ substrate by CSD method have been discussed. The microstructure of ZNMO films is examined by x-ray diffraction and FESEM. The intensities of XRD peaks of the ZNMO films decrease with increasing Zn concentration, and the samples have similar surface morphology. The optical constants (n, κ) of ZNMO films with different Zn concentration have been investigated by spectroscopic ellipsometric in the wavelength range of 300 ~ 1100 nm. As the Zn concentration increases, the refractive index n of the samples changes erratically due to the effects of electronic band structure, crystallinity and thickness. The extinction coefficient κ of ZNMO films (except $x=0.2$) decreases with increasing Zn concentration in wavelength range of 510 ~ 900 nm.

The effect of cation configuration and lattice strain caused by Zn substituting has been observed on the Raman spectra. Our studies indicate that the structural and optical properties of ZNMO films have close relationship with the Zn concentration, which might have potential application in optoelectronic devices.

Acknowledgements

This work was supported by National Natural Science Foundation of China(61275111 , 11304336), and Shanghai Project (15ZR1445700).

References

[1] Feteira A. Negative temperature coefficient resistance (NTCR) ceramic thermistors: an industrial perspective [J]. *J. Am. Ceram. Soc.*, 2009, **92**(5):967-983.

[2] Park K, Microstructure and electrical properties of $Ni_{1.0}Mn_{2-x}Zr_xO_4$ ($0 \leqslant x \leqslant 1.0$) negative temperature coefficient thermistors [J]. *Mater. Sci. Eng.*, B, 2003, **104**(1-2):9-14.

[3] Ryu J, Park D S, Schmidt R. In-plane impedance spectroscopy in aerosol deposited $NiMn_2O_4$ negative temperature coefficient thermistor films [J]. *J. Appl. Phys.*, 2011, **109**(11):113722.

[4] Fritscha J S S, Brieua M, Couderc J J, *et al*. Correlation between the structure, the microstructure and the electrical properties of nickel manganite negative temperature coefficient (NTC) thermistors [J]. *Solid State Ionics*, 1998, **109**(s3-4): 229-237.

[5] Aleksic O S, Nikolic M V, Lukovic M D, *et al*. Preparation and characterization of Cu and Zn modified nickel manganite NTC powders and thick film thermistors [J]. Mater. Sci. Eng., B, 2013, **178**(3):202-210.

[6] Åsbrink S, Wa´skowska A, Drozd M, *et al*. Physical properties and X-ray diffraction of a $NiMn_2O_4$ single crystal below and above the ferrimagnetic transition at Tc = 145 K [J]. *J. Phys. Chem. Solids*, 1997, **58**(5):725-729.

[7] Schmidt R, Basu A, Brinkman A W, *et al*. Electron-hopping modes in $NiMn_2O_{4+\delta}$ materials [J]. *Appl. Phys. Lett.*, 2005, 86(7); 073501.

[8] Wei S H, Zhang S B. First-principles study of cation distribution in eighteen closed-shell $A^{II}B_2^{III}O_4$ and $A^{IV}B_2^{II}O_4$ spinel oxides[J]. *Phys Rev B*, 2001, **63**(4):045112.

[9] Baykal A, Güner S, Demir A, *et al*. Effect of zinc substitution on magneto-optical properties of $Mn_{1-x}Zn_xFe_2O_4/SiO_2$ nanocomposites [J]. *Ceram. Int.*, 2014, **40**(8): 13401-13408.

[10] Buvaneswari G, Aswathy V, Rajakumari R. Comparison of color and optical absorbance properties of divalent ion substituted Cu and Zn aluminate spinel oxides synthesized by combustion method towards pigment application [J]. *Dyes Pigments*, 2015, **123**:413-419.

[11] Mukherjee K, Kumar K, Banerjee A. Observation of different spin behavior with temperature variation and Cr substitution in a multiferroic compound YMn_2O_5 [J]. *Solid State Commun*, 2013, **153**(1):66-70.

[12] Park K, Lee J K, Kim S J, *et al*. The effect of Zn on the microstructure and electrical properties of $Mn_{1.17-x}Ni_{0.93}Co_{0.9}Zn_xO_4$ ($0 \leqslant x \leqslant 0.075$) NTC thermistors [J]. *Journal of Alloys and Compounds*, 2009, **467**(1-2):310-316.

[13] Wei Q M, Li J B, Chen Y J, *et al*. X-ray study of cation distribution in $NiMn_{1-x}Fe_2$-xO_4 ferrites [J]. *Mater Charact*, 2001, **47**(3-4):247-252.

[14] Cheng F, Wang J, Zhang H, *et al*. Phase transition and electrical properties of $Ni_{1-x}Zn_xMn_2O_4$ ($0 \leqslant x \leqslant 1.0$) NTC ceramics [J]. *J. Mater. Sci. Mater. Electron.*, 2014, **26**(3):1374-1380.

[15] Takahashi J, Miura A, Itoh H, *et al*. Phase change and electrical resistivity of Zn-Mn-Ni-O-based NTC thermistors produced using IZC powder recycled from used dry batteries [J]. Ceram. Int., 2008, **34**(4):853-857.

[16] Chanel C, Guillemet-Fritsch S, Sarrias J, *et al*. Microstructure and electrical properties of Ni-Zn manganite ceramics [J]. *Int J Inorg Mater*, 2000, **2**(2-3):241-247.

[17] Guillemet-Fritsch S, Baudour J L, Chanel C, *et al*. X-ray and neutron diffraction studies on nickel zinc manganite $Mn_{2.35-x}Ni_{0.65}Zn_xO_4$ powders [J]. *Solid State Ionics*, 2000, **132**(1-2):63-69.

[18] Zhao C, Zhao Y, Wang Y. Annealing on the electrical properties of $Ni_{0.75}Mn_{2.25}O_4$ and $Zn_{0.8}Ni_{0.75}Mn_{1.45}O_4$ NTC ceramics[J]. *Solid State Commun*, 2012, **152**(7): 593-595.

[19] Zhang L B, Hou Y, Zhou W, *et al*. Investigation on optical properties of $NiMn_2O_4$ films by spectroscopic ellipsometry [J]. *Solid State Commun*, 2013, **159**:32-35.

[20] Zhao C, Wang B, Yang P, *et al*. Effects of Cu and Zn co-doping on the electrical properties of $Ni_{0.5}Mn_{2.5}O_4$ NTC ceramics [J]. *J. Eur. Ceram. Soc.*, 2008, **28**(1):35-40.

[21] Fujiwara H, Kondo M. Effects of carrier concentration on the dielectric function of ZnO:Ga and In_2O_3:Snstudied by spectroscopic ellipsometry: Analysis of free-carrier and band-edge absorption [J]. *Phys Rev B*, 2005, **71**(7):075109.

[22] Jellison G E, Modine F A. Parameterization of the optical functions of amorphous materials in the interband region [J]. *Appl. Phys. Lett.*, 1996, **69**(3):371.

[23] Ye C, Pan S S, Teng X M, *et al*. Preparation and optical properties of nanocrystalline thin films in the ZnO-TiO_2 system [J]. *Appl. Phys. A*, 2007, **90**(2):375-378.

[24] Hu Z, Wang G, Huang Z, *et al*. Optical properties of $Bi_{3.25}La_{0.75}Ti_3O_{12}$ thin films using spectroscopic ellipsometry [J]. *J. Appl. Phys.*, 2003, **93**(7):3811.

[25] Hou Y, Xue J, Huang Z, *et al*. Structure-related optical properties of $Bi_{4-x}La_xTi_3O_{12}$ thin films grown on Pt/Ti/SiO_2/Si substrate [J]. *Thin Solid Films*, 2008, **517**(2): 901-904.

[26] Hu Z, Wang G, Huang Z, *et al*. Effects of thickness on the infrared optical properties of $Ba_{0.9}Sr_{0.1}TiO_3$ ferroelectric thin films [J]. *Appl Phys A-mater*, 2004, **78**(5):757-760.

[27] Lakhdar M H, Ouni B, Amlouk M. Thickness effect on the structural and optical constants of stibnite thin films prepared by sulfidation annealing of antimony films [J]. *Optik: Int. J. Light Electron Opt.*, 2014, **125**(10):2295-2301.

[28] Julien C, Massot M, Rangan S, *et al*. Study of structural defects in γ-MnO_2 by Raman spectroscopy [J]. *J. Raman Spectrosc.*, 2002, **33**(4):223-228.

[29] Ma C, Ren W, Wang L, *et al*. Effects of cation distribution on optical properties of Mn-Co-Ni-O films [J]. *Mater. Lett.*, 2015, **153**:162-164.

[30] Wei Y, Nam K, Kim K, *et al*. Spectroscopic studies of the structural properties of Ni substituted spinel $LiMn_2O_4$ [J]. *Solid State Ionics*, 2006, 177(1-2):29-35.

[31] Chaturvedi A, Sathe V. Thickness dependent Raman study of epitaxial $LaMnO_3$ thin films [J]. *Thin Solid Films*, 2013, **548**:75-80.

[32] Seong M J, Chun S H, Cheong H M,*et al*. Spectroscopic determination of hole density in the ferromagnetic semiconductor $Ga_{1-x}Mn_xAs$ [J]. *Phys Rev B*, 2002, **66**(3):033202.

[33] Steele J A, Lewis R A, Henini M, *et al*. Raman scattering studies of strain effects in (100) and (311) B $GaAs_{1-x}Bi_x$ epitaxial layers [J]. *J. Appl. Phys.*, 2013, **114**(19):193516.